ELSEVIER

Journal of Alloys and Compounds 218 (1995) 101–109

Journal of ALLOYS AND COMPOUNDS

# Crystal structure, phase abundance and electrode performance of Laves phase compounds (Zr, A)$V_{0.5}Ni_{1.1}Mn_{0.2}Fe_{0.2}$ (A≡Ti, Nb or Hf)

J. Huot [a], E. Akiba [a], T. Ogura [b], Y. Ishido [b]

[a] *National Institute of Materials and Chemical Research, 1-1, Higashi, Tsukuba, Ibaraki 305, Japan*

[b] *Shin-Kobe Electric Machinery Co. Ltd., Okabe-machi, Osato-gun, Saitama 369-02, Japan*

(Received 6 May, 1994; in final form 17 August, 1994)

**Abstract**

The variation in crystal structure with substitution of the Zr site of $ZrM_2$ ($M_2 \equiv V_{0.5}Ni_{1.1}Mn_{0.2}Fe_{0.2}$) by Ti, Nb or Hf has been studied. The C14 and C15 Laves phases coexist for all alloys except $TiM_2$ (b.c.c.), $Zr_{0.25}Ti_{0.75}M_2$ (87% C14 and 13% b.c.c.), $Zr_{0.5}Ti_{0.5}M_2$ and $NbM_2$ (pure C14). The C15 phase cannot accommodate an M site–M site bond distance of less than 2.46 Å. The phase stability under hydriding is confirmed. The pressure–composition isotherm measurements show that the multiphase alloys behave as a single phase. Also, the b.c.c. phase alloy $TiM_2$ can absorb hydrogen. For electrode performances, it is observed that the alloys with the C15 phase present a large reduction in discharge capacity when the discharge current is increased. For the alloys composed of only the C14 phase, the discharge capacity does not change significantly when the discharge current is increased.

*Keywords:* Crystal structure; Phase abundance; Electrode performance; Laves phase compounds

## 1. Introduction

Because of the wide variety of practical applications [1], many kinds of hydrogen-absorbing alloy have recently been developed. For battery application, most of the work has been done on $AB_5$-type alloys [2,3], and Ti–Zr–Ni-based alloys [4]. However, because of their potentially higher discharge capacities, Laves phase $AB_2$-type alloys are now being investigated [5,6] as the electrode material of possible replacement for the toxic Ni–Cd battery.

Laves phases are intermetallic compounds in which a strong hydride former occupies the A site and a weaker hydride former is on the B site. Three crystal structures typified the Laves phases, they are (i) hexagonal C14 ($MgZn_2$ type), (ii) cubic C15 ($MgCu_2$ type) and (iii) hexagonal C36 ($MgNi_2$ type).

In all these structures, the A atom is surrounded by four A and twelve B atoms and the B atom is surrounded by six A and six B atoms. The difference between these structures is explained by the different stackings of the hexagonal layers [7]. Laves phase structures are determined primarily by the size factor [8], but the electron-to-atom ratio also plays a crucial role in the appearance of a particular structure [9]. For metal hydride applications, the most frequent structures are the C14 and C15 phases [10].

Recently there have been indications that multiple-phase compounds are good materials for battery applications [11]. However, to our knowledge, no precise determination of phase abundance for metal hydride alloys has been reported. Such information is indispensable for the comprehension of the multiphase effect on hydride properties. In this work, we studied the effect of the phase abundance on the electrode performance.

In $AB_2$-type Laves phase alloys, many attempts have been made to modify the B site metals with the A site fixed [12–16]. However, reports on A site modifications are relatively rare [7,17,18]. Therefore we decided to investigate the effect on phase abundance when substitution is on the A site. For this purpose, we selected the system $Zr_{1-x}A_xM_2$ ($M_2 \equiv V_{0.5}Ni_{1.1}Mn_{0.2}Fe_{0.2}$) where A≡Ti, Nb or Hf and $x = 0$, 0.25, 0.50, 0.75, 1.00.

We used the Rietveld refinement method to determine the crystal structure and to estimate the phase abun-


*SSDI* 0925-8388(94)01370-5

dance. For all alloys, the electrode performance was measured and compared with the theoretical discharge capacity computed from measured pressure–composition (PC) isotherms.

## 2. Experimental

All raw metals were at least 99.9% pure except for Hf (purity, 99%). The alloys were produced by arc melting on a water-cooled copper crucible under an argon atmosphere. During preparation, the alloys were turned over four times to ensure homogeneity. The PC isotherms were measured with a conventional constant-volume apparatus [19]. Before PC isotherm measurements, the alloys were pretreated by evacuating at 773 K and introducing hydrogen into the alloys at room temperature. A Rigaku diffractometer with a Cu K$\alpha$ radiation was used for powder X-ray diffraction measurements. The diffraction pattern was analyzed by the Rietveld method, using RIETAN software [20]. The electrodes were prepared by mixing 0.2 g of the alloy powder (200 mesh) with 0.8 g of Ni powder (200 mesh). The mixture was pressed into a disk (10 mm diameter and 1.5 mm thickness) and then compressed between two sponge nickel plates. Two Ni cathodes which have sufficiently high capacities were attached to both sides of the alloy electrode. An electrolyte solution of 30 wt.% KOH was used. Discharge capacities of the fully charged alloy electrodes were measured at 293 K, with discharge currents of 70 and 20 mA (g alloy)$^{-1}$. For both discharge currents, the cut-off voltage was 0.8 V.

## 3. Results

### 3.1. X-ray powder diffraction

For a precise determination of crystal structure, the powder diffraction pattern of all alloys, except $TiM_2$, were analyzed by the Rietveld method [20]. The X-ray diffraction pattern of $Zr_{0.75}Ti_{0.25}M_2$ is shown in Fig. 1. The upper curve and dots are the calculated and experimental powder diffraction data respectively. The lower curve ($\Delta Y$) is the difference between the measured and calculated profiles. Two small parts of the powder diffraction pattern were deleted because they contain small peaks from an unknown third phase. Because it is impossible to identify this third phase, these peaks were removed from Rietveld refinement. The calculated Bragg reflections for each phase are indicated by small bars in Fig. 1. Most of the Bragg reflections of the C15 phase are superposed by peaks coming from the C14 phase. Therefore only by using the Rietveld refinement method can both phases be distinguished. Considering that some parts of the powder diffraction pattern were deleted and that the $R$ values are not very small, the phase abundance can only be estimated from the Rietveld refinement results.

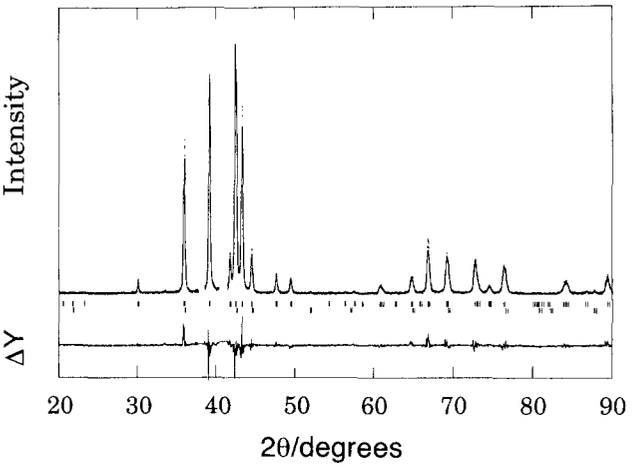


Fig. 1. X-ray powder diffraction pattern fitting by Rietveld refinement of $Zr_{0.75}Ti_{0.25}M_2$. The short vertical bars indicate the centers of Bragg reflections; the upper row is for C14, and the bottom row is for C15.

In the Rietveld method, various $R$ values are used to investigate the goodness of the fit. The most meaningful are the "$R$-weighted pattern" $R_{wp}$ which measures the weighted difference between the calculated and measured intensities, the "$R$ expected" value $R_e$ is an estimation of the minimum possible value of $R_{wp}$ and the "$R$ Bragg factor" $R_B$ which is a measure of the difference between the calculated and "experimental" intensities of Bragg reflections. The definitions of these quantities are in the literature [21,22]. A reliable indicator of the goodness of the fit is the quantity $S = R_{wp}/R_e$ [21].

The crystallographic data for $Zr_{0.75}Ti_{0.25}M_2$ are presented in Table 1. Considering the low background intensity and the sharpness of the peaks, the reported $S$ value of 1.63 is quite satisfactory [23]. If the region omitted owing to the unknown third phase is included in the refinement, $R_{wp}$ increases to 14.09%, $S$ is 1.87 and $R_B$ decreases to 5.17% for the C14 phase and to 5.40% for the C15 phase.

In Table 2 we present the $R$ values for all alloys. Most of the alloys present a mixture of two major phases. For some alloys, a third phase was also observed. For the $Zr_{1-x}Ti_xM_2$ and $Zr_{1-x}Nb_xM_2$ systems, the $R_{wp}$ values decrease by about 10% when these unknown phases are eliminated from the refinement calculation. However, for the system $Zr_{1-x}Hf_xM_2$ the unknown phase is more important. In that case, the $R_{wp}$ values decrease by 30–45% when the unknown phase is removed from the calculation.

### 3.2. Phase abundance

Recently [24] it has been shown that the Rietveld method can be useful for phase abundance determi-

Table 1
Crystal structure refinement results for $Zr_{0.75}Ti_{0.25}M_2$ (M(1)≡$Zr_{0.75}Ti_{0.25}$; M(2)≡$V_{0.25}Ni_{0.55}Mn_{0.1}Fe_{0.1}$), where the values in parentheses are one standard deviation and refer to the last digit and where the space group sequence number is in parentheses

| Phase | Space group | $R_B$ (%) | Scale factor ($\times 10^4$) | Lattice parameters (Å) | Atom | Wyckoff symbol | Refined coordinates | Thermal parameter |
|---|---|---|---|---|---|---|---|---|
| C14 | $P6_3/mmm$ (No. 194) | 6.63 | 3.82(4) | $a=4.9842(3)$ $c=8.1339(4)$ | M(1) | 4f | $z=0.064(1)$ | 1.0(3) |
| | | | | | M(2) | 2a | | 1.0(5) |
| | | | | | M(2) | 6h | $x=0.830(1)$ | 1.0(4) |
| C15 | $Fd\bar{3}m$ (No. 227) | 6.21 | 0.092(6) | $a=7.0269(4)$ | M(1) | 8a | | 1(1) |
| | | | | | M(2) | 16d | | 1(2) |

Fitting parameters: $R_{wp}=12.26\%$; $S=1.63$.

Table 2
$R$ values obtained from the Rietveld refinement method: $S=R_{wp}/R_e$

| Alloy | $R_{wp}$ | $S$ | Phase | Amount (%) | $R_B$ |
|---|---|---|---|---|---|
| $ZrM_2$ | 17.16 | 2.25 | C14 | 57(1) | 7.90 |
| | | | C15 | 43(1) | 9.50 |
| $Zr_{0.75}Ti_{0.25}M_2$ | 12.26 | 1.63 | C14 | 91(1) | 6.63 |
| | | | C15 | 8.7(5) | 6.21 |
| $Zr_{0.5}Ti_{0.5}M_2$ | 17.00 | 1.96 | C14 | 100 | 6.27 |
| $Zr_{0.25}Ti_{0.75}M_2$ | 17.89 | 2.00 | C14 | 87(1) | 12.66 |
| | | | b.c.c. | 13.2(6) | 10.24 |
| $Zr_{0.75}Nb_{0.25}M_2$ | 23.74 | 2.95 | C14 | 73.8(9) | 14.68 |
| | | | C15 | 26.2(6) | 18.64 |
| $Zr_{0.5}Nb_{0.5}M_2$ | 20.07 | 2.07 | C14 | 79.1(9) | 10.79 |
| | | | C15 | 20.9(8) | 14.95 |
| $Zr_{0.25}Nb_{0.75}M_2$ | 26.02 | 2.77 | C14 | 89.8(9) | 12.36 |
| | | | C15 | 10.2(8) | 13.78 |
| $NbM_2$ | 25.34 | 2.89 | C14 | 100 | 12.83 |
| $Zr_{0.75}Hf_{0.25}M_2$ | 15.72 | 1.87 | C14 | 77.4(9) | 7.15 |
| | | | C15 | 22.6(8) | 7.71 |
| $Zr_{0.5}Hf_{0.5}M_2$ | 14.67 | 1.82 | C14 | 85(1) | 6.85 |
| | | | C15 | 14.5(8) | 5.70 |
| $Zr_{0.25}Hf_{0.75}M_2$ | 18.49 | 2.57 | C14 | 81.4(9) | 10.79 |
| | | | C15 | 18.5(7) | 15.57 |
| $HfM_2$ | 16.65 | 2.07 | C14 | 86.5(9) | 8.65 |
| | | | C15 | 13.5(8) | 8.12 |

nation. From the refined parameters, the abundance of each phase is calculated from the relation

$$W_i = S_i D_i V_i^2 / \sum_j (S_j D_j V_j^2) \quad (1)$$

where $S_i$, $D_i$ and $V_i$ are the scale factor, theoretical density and volume respectively of phase $i$. These parameters are automatically given in the output of Rietveld refinement. Therefore it is easy to calculate the phase abundance. However, the scale factor given by the RIETAN software is not equal to the scale factor of Eq. (1). The scale factor should be corrected as $S=S_R/c^2$ where $S_R$ is the scale factor given by RIETAN. The value of the factor $c$ depends on the position of the centering site in the unit cell and on the presence or not of a center of symmetry. For the b.c.c. and C15 phases, $c=4$ and, for the C14 phase, $c=2$. To avoid confusion, in this paper we report only the corrected scale factors $S$. In Table 3 we present, in detail, the calculation for the compound $Zr_{0.5}Ti_{0.75}M_2$. The uncertainties in the density and volume are not quoted, because they are negligible compared with the uncertainty on the scale factor. As seen in Table 3, the densities of both phases are very similar. However, the C14 phase unit-cell volume is about six times the b.c.c. unit-cell volume. Because the unit-cell volume is quadratic in the phase abundance Eq. (1), for that particular case the volume of each phase is the dominant factor.

The amount of the hexagonal C14 phase in each alloy is presented in Fig. 2. The cubic C15 phase makes up the rest of the alloys except for $TiM_2$ (100% b.c.c.) and $Zr_{0.25}Ti_{0.75}M_2$ (87% C14 and 13% b.c.c.).

In the compounds $Zr_{1-x}Hf_xM_2$, the zirconium atom is replaced by an atom having the same valence and with almost the same Goldschmidt radius [25] (1.60 Å for Zr and 1.59 Å for Hf). However, the amount of the C14 phase goes from 57% for $ZrM_2$ to 87% for $HfM_2$. This indicates that the type of Laves phase formed is not determined by the geometry nor by the electron-to-atom ratio.

The compounds $Zr_{1-x}Nb_xM_2$ present an increase in the amount of the C14 phase from 57% for $ZrM_2$ to 100% for $NbM_2$. This shows that both phases can coexist for a wide range of $x$ values.

Table 3
Parameters used in the phase abundance calculation for the compound $Zr_{0.25}Ti_{0.75}M_2$, where $S$, $D$ and $V$ are the scale factor, calculated density and unit-cell volume respectively and the phase abundance is calculated from Eq. (1).

| Phase | $S(\times 10^4)$ | $D$ (g cm$^{-3}$) | $V(\times 10^{23})$ (cm$^3$) | $SDV^2(\times 10^{47})$ (g cm$^3$) | Abundance (%) |
|---|---|---|---|---|---|
| C14 | 4.24(6) | 6.768 | 16.597 | 7.9(1) | 87(1) |
| B.c.c. | 23.7(9) | 6.901 | 2.713 | 1.20(5) | 13.2(6) |

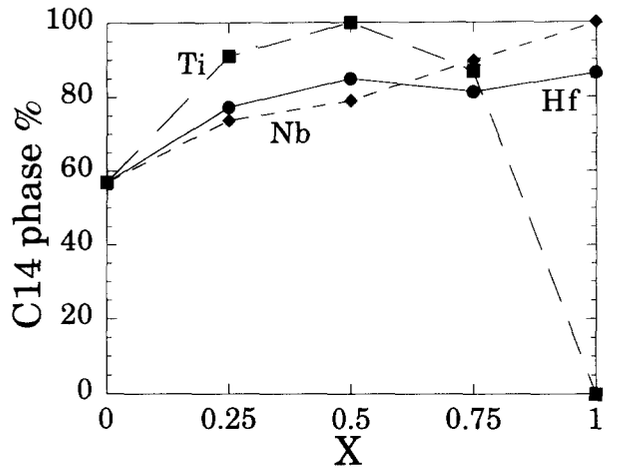


Fig. 2. Proportion of the C14 phase in $Zr_{1-x}A_xM_2$ alloys (A≡Ti, Nb or Hf).

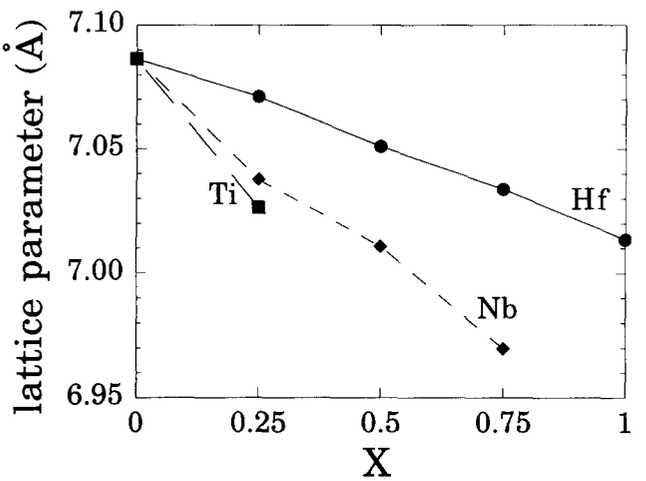


Fig. 3. Lattice parameter of the cubic C15 phase.

A very interesting behavior is shown by the compounds $Zr_{1-x}Ti_xM_2$. The amount of C15 decreases rapidly with increasing $x$ to reach the pure C14 phase at $x=0.5$. For $x=0.75$ ($Zr_{0.25}Ti_{0.75}M_2$), the alloy has a b.c.c. phase (13%) and a C14 phase (87%). The alloy $TiM_2$ is pure b.c.c. It should be pointed out that, in the present systems, the three phases C14, C15 and b.c.c. never appear simultaneously.

### 3.3. Lattice parameters

For all alloys, the lattice parameters were determined by the Rietveld method. The only exception is the b.c.c. alloy $TiM_2$. For this alloy, only the 110 reflection was used to calculate the lattice parameter ($a=2.963$ Å).

The lattice parameters of the cubic C15 phase are presented in Fig. 3. For the systems $Zr_{1-x}Hf_xM_2$ and $Zr_{1-x}Nb_xM_2$, the lattice parameters decrease linearly with increasing $x$. If we assume such a linear decrease for $Zr_{1-x}Ti_xM_2$, we can calculate the "expected" lattice parameter for a possible C15 cubic phase for the alloy $Zr_{0.5}Ti_{0.5}M_2$. This calculated value ($a=6.965$ Å) seems to be the lower bound beyond which the C15 phase cannot exist. Such a lower bound is also observed for the compounds $Zr_{1-x}Nb_xFe_2$ [7] and $Zr_{1-x}Ti_xFe_2$ [26]. The lower bounds are 6.996 Å for the former and 6.98 Å for the latter. Before investigating the possible reason for this lower bound, we should examine the lattice parameters of the C14 phase.

The lattice parameters of the hexagonal C14 phase are presented in Fig. 4. Because Zr and Hf atoms are very similar in size, the compound $Zr_{1-x}Hf_xM_2$ shows a very small decrease in lattice parameter. The compounds $Zr_{1-x}Nb_xM_2$ and $Zr_{1-x}Ti_xM_2$ have almost identical decreases in lattice parameters with increasing $x$. This situation is probably caused by their identical Goldschmidt radii (1.47 Å). However, these two systems do not show the same behavior because $TiM_2$ is pure b.c.c. while $NbM_2$ is pure C14. In that regard, pertinent information is given by the ratio $c/a$ of lattice parameters. This ratio is shown in Fig. 5. From Fig. 5, we see that the ratio $c/a$ drops more rapidly for $Zr_{1-x}Ti_xM_2$ than for the other two systems.

With the values of lattice parameters and atomic positions for the C14 and C15 phases, we can now

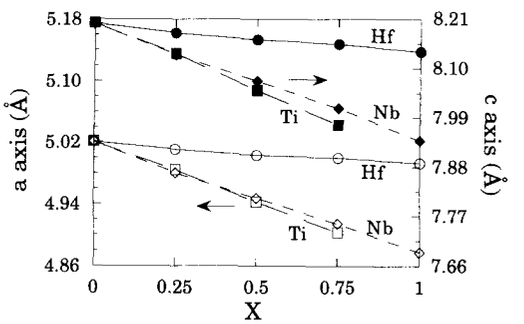


Fig. 4. Lattice parameters of the hexagonal C14 phase for the compounds $Zr_{1-x}A_xM_2$ (A≡Hf, Nb or Ti): ○, ●, Hf; □, ■, Ti; ◇, ◆, Nb; ○, □, ◇, $a$ axis; ●, ■, ◆, $c$ axis.

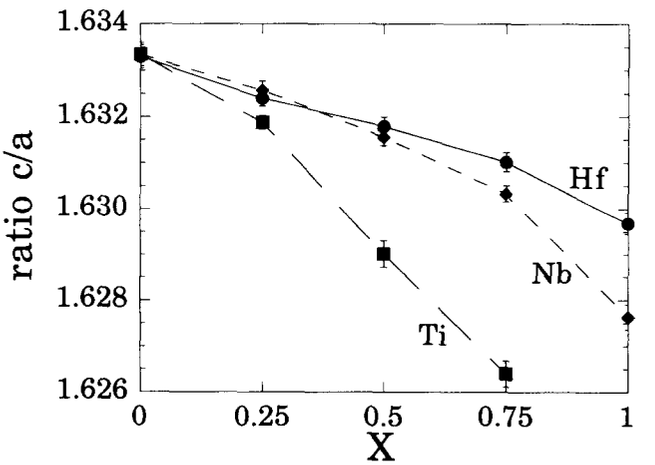


Fig. 5. Lattice parameter ratio $c/a$ for the hexagonal C14 phase of the compounds $Zr_{1-x}A_xM_2$ (A≡Hf, Nb or Ti).

investigate the reasons for the disappearance of the C15 phases for certain compounds. As stated before, the Laves phase structures are primarily determined by size factors. In that regard, in Fig. 6, we plotted the shortest interatomic distance. For both C14 and C15 phases, this is the distance between two M atoms (M–M distance). For the C14 phase, this is the distance between two atoms on 6h sites (Wyckoff notation). Fig. 6 clearly shows that in the C15 phase the M–M distance cannot be less than 2.46 Å. On the contrary, for the C14 phase, the M–M distance is 2.42 Å on average. It is well known that contacts between atoms are possible in Laves phase structures. Therefore, let us define the amount of compression as

$$C_{MM} = \left(1 - \frac{d_{MM}}{2r_M}\right)100 \quad (2)$$

where $r_M$ is the Goldschmidt radius of an M site atom, $d_{MM}$ is the interatomic distance between two M atoms and $C_{MM}$ is the compression in per cent. In the present system, we took $r_M$ as the stoichiometrically weighted sum of the Goldschmidt radii of atoms forming the M site (1.2675 Å). We think that this average procedure is justified because in Laves phases it is all atoms jointly that determine all interatomic distances [27].

For the C15 phase, a minimum distance of 2.46 Å means a compression factor $C_{MM}$ of 3.0%. This is slightly smaller than the compression factor of the C15 prototype $Cu_2Mg$ ($C_{CuCu}$ = 3.5%). On the contrary, on average, the C14 phase has $C_{MM}$ = 4.5%. For the C14 prototype ($MgZn_2$) the compression is larger ($C_{ZnZn}$ = 7.6%). Therefore for the present system the M site atoms cannot be compressed by more than 3.0% in the C15 phase while the C14 phase can accommodate larger compression.

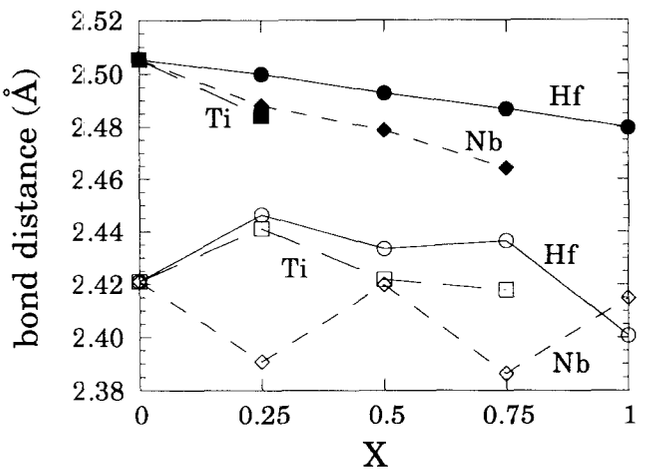


Fig. 6. Shortest interatomic distance between two B site atoms: ○, ●, Hf; □, ■, Ti; ◇, ◆, Nb; ○, □, ◇, C14 phase; ●, ■, ◆, C15 phase. For clarity, the error bars are omitted. For C15 phase, the error bar is 0.0002. For C14 phase, because of the uncertainty in atomic position, the error bar is much larger (0.020).

### 3.4. Phase stability

In order to discuss the relation between crystal structure and electrode performance, the crystal structure stability under hydriding must be investigated. For this purpose, we selected the alloys $ZrM_2$, $Zr_{0.75}Ti_{0.25}M_2$ and $Zr_{0.5}Ti_{0.5}M_2$.

For these alloys, one part of each of the as-cast alloys was fully hydrided and then dehydrided. Rietveld refinement was performed in the same way as for the as-cast alloys. The results are shown in Table 4.

Table 4 shows that the lattice parameters of both C14 and C15 phases do not vary significantly under hydriding. Moreover, there is no change in phase abundance. In a powder diffraction pattern, the peak shape is the convolution of an instrumental aberration function and a specimen profile-broadening function. The specimen broadening function is mainly due to crystallite size and microstrain effects [28]. Therefore, by comparing the full width at half-maximum (FWHM) of X-ray diffraction peaks, we can obtain information about the relative crystallite size and microstrain of the different samples. For this purpose, we have selected the 103 reflection of the C14 phase. This particular reflection is chosen because it is one of the most intense peaks and it does not overlap with any C15 reflection lines. From Table 4, we see that there is no variation in FWHM after hydriding. This indicates that all samples investigated have the same crystallite size and microstrain.

No variation in lattice parameters, phase abundance and FWHM indicates that both C14 and C15 phases are stable under hydriding. The consistency of phase abundance also denotes no disproportion or phase decomposition under hydrogenation.

### 3.5. Pressure–composition isotherms

The PC dependence was measured at 293, 313 and 353 K for every alloy with the exception of $NbM_2$. We do not report the PC curve for $NbM_2$ because, up to 6 MPa, this alloy is a very poor hydrogen absorber. In Fig. 7 we present the compound $Zr_{0.75}Hf_{0.25}M_2$ as representative of PC measurements. One can see that, as the temperature increases, the hydrogen-to-metal atom ratio [H]/[M] decreases. For every alloy, there is no well-defined plateau at any isotherms. Because of this absence of a plateau in the PC curves, it is impossible to determine the heat of hydride formation.

The hydrogen equilibrium pressure as a function of [H]/[M] for the desorption side of the systems $Zr_{1-x}Hf_xM_2$, $Zr_{1-x}Nb_xM_2$ and $Zr_{1-x}Ti_xM_2$ at 313 K are presented in Fig. 8. The desorption isotherm is chosen because it is less dependent on experimental conditions. All curves in Fig. 8 are smooth, showing no double plateau or kinks. However, most of these alloys are

Table 4
Lattice parameters and phase composition of $Zr_{1-x}Ti_xM_2$ for $x \leq 0.5$, where the values in parentheses are the values of one standard deviation in the last digits and where the full width at half-maximum is for the reflection line 103

| Alloy | | C14 | | | | C15 | |
|---|---|---|---|---|---|---|---|
| | | *a* (Å) | *c* (Å) | Abundance (%) | 103 FWHM (°) | *a* (Å) | Abundance (%) |
| $ZrM_2$ | As cast | 5.0212(4) | 8.2014(6) | 57(1) | 0.18 | 7.0865(4) | 43(1) |
| | Dehydrided | 5.0213(2) | 8.2031(3) | 53.6(5) | 0.18 | 7.0875(2) | 46.3(6) |
| $Zr_{0.75}Ti_{0.25}M_2$ | As cast | 4.9842(3) | 8.1340(4) | 91(1) | 0.22 | 7.0269(4) | 8.7(6) |
| | Dehydrided | 4.9858(3) | 8.1351(4) | 88.7(4) | 0.22 | 7.0290(4) | 11(1) |
| $Zr_{0.5}Ti_{0.5}M_2$ | As cast | 4.9425(5) | 8.0514(7) | 100 | 0.32 | | |
| | Dehydrided | 4.9428(3) | 8.0505(4) | 100 | 0.28 | | |

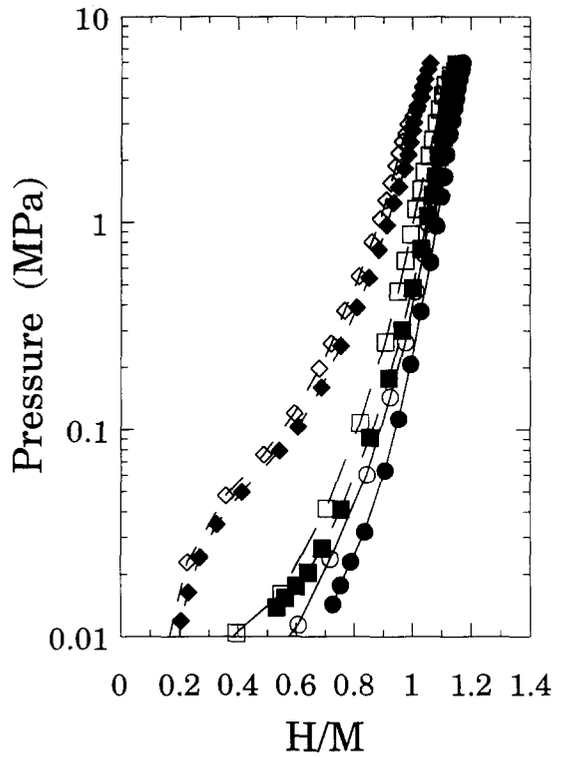


Fig. 7. PC isotherms of the $Zr_{0.75}Hf_{0.25}M_2$–$H_2$ system: ●, ○, 20 °C; ■, □, 40 °C; ♦, ◇, 80 °C; ○, □, ◇, absorption; ●, ■, ♦, desorption.

multiphase. To investigate the possibility that one phase absorbs hydrogen while another does not, we consider the alloy $ZrM_2$ ($x=0$ on the figure). This alloy is composed of 57% of C14 phase and 43% of C15 phase. The asymptotic value of [H]/[M] is 1.2. If we assume that only the C14 phase absorbs hydrogen, this phase should have [H]/[M] = 2.1. In the same way, if only the C15 phase absorbs hydrogen then [H]/[M] = 2.8 for that phase. These [H]/[M] values are higher than those of any other Laves phase alloys [10]. Furthermore, according to the Schoemaker–Schoemaker [29] exclusion rule, the upper limit of [H]/[M] is 2.0 for C15 phase and 2.1 for C14 phase. We therefore conclude that both phases could absorb hydrogen. These multiphase alloys absorb hydrogen in the same way as a single-phase alloy does.

In the system $Zr_{1-x}Nb_xM_2$ (Fig. 8(b)) the ratio [H]/[M] decreases with increasing $x$. The compound $NbM_2$ does not absorb hydrogen up to 5 MPa. As stated earlier, in Laves phases the A site atom has to be a strong hydride former. Because the niobium hydride capacity ($NbH_{0.5}$) is less than zirconium ($ZrH_2$), it is understandable that by replacing zirconium by niobium on the A site the hydrogen capacity of the alloy decreases.

The system $Zr_{1-x}Hf_xM_2$ (Fig. 8(c)) shows a small decrease in [H]/[M] with increasing $x$. Hafnium has the same capacity ($HfH_2$) as zirconium, but zirconium hydride is more stable than hafnium hydride ($-82$ kJ (mol H)$^{-1}$ for $ZrH_2$ compared with $-66$ kJ (mol H)$^{-1}$ for $HfH_2$) [30]. This may explain the decrease in [H]/[M] when zirconium is replaced by hafnium.

The system $Zr_{1-x}Ti_xM_2$ shows a very interesting behavior. From Fig. 8(a), we see that for $x=0$ and $x=0.25$ the general shape of the curves is the same as for the system $Zr_{1-x}Hf_xM_2$. This could be expected because the heat of formation of $TiH_2$ ($-68$ kJ (mol H)$^{-1}$) is almost the same as that of $HfH_2$. At $x=1$ ($TiM_2$), the alloy is pure b.c.c. However, that b.c.c. phase can also absorb hydrogen. The shape of the PC curve of the pure b.c.c. alloy $TiM_2$ is quite different from that of the other PC curves.

### 3.6. Electrode performance

Having determined the crystal structure and PC isotherms of the alloys, we now analyze the actual and theoretical electrode performances with respect to the crystal structure. The measured discharge capacity of the alloys is shown in Fig. 9. At a low discharge current (20 mA (g-alloy)$^{-1}$) the alloy $ZrM_2$ has the highest capacity. This is also the alloy with the highest proportion of C15 phase. The effect of substituting Hf, Ti or Nb for Zr is to reduce the discharge capacity linearly with increasing $x$. For $x=0$ and $x=0.25$ these alloys compare

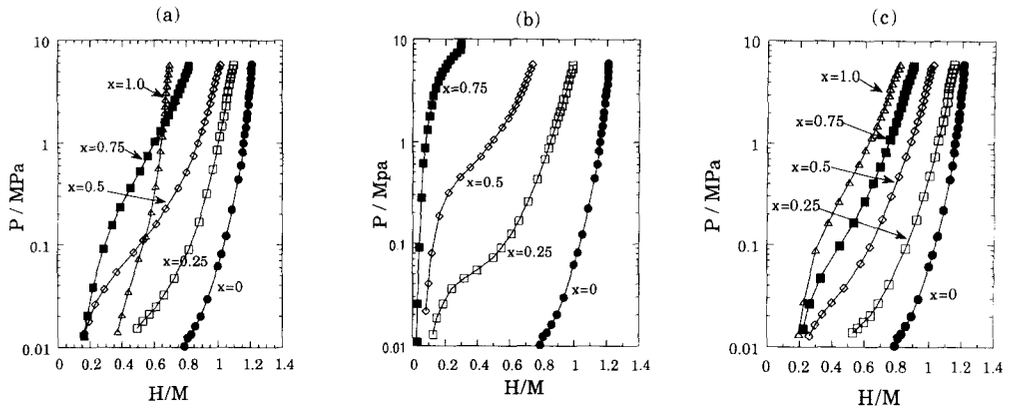


Fig. 8. Desorption PC diagrams of $Zr_{1-x}A_xM_2$–$H_2$ systems at 313 K: (a) $Zr_{1-x}Ti_xM_2$; (b) $Zr_{1-x}Nb_xM_2$; (c) $Zr_{1-x}Hf_xM_2$.

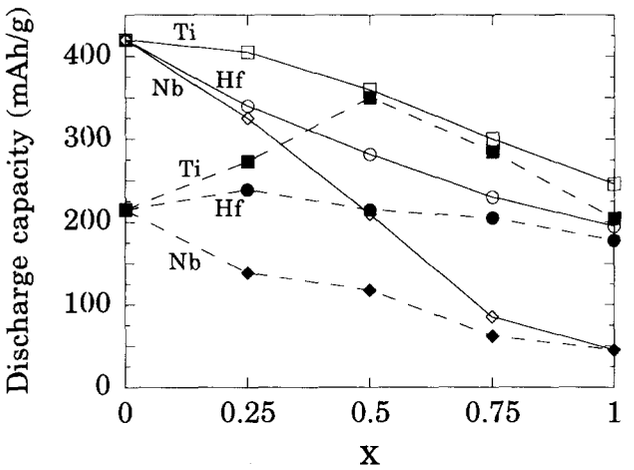


Fig. 9. Discharge capacity of $Zr_{1-x}A_xM_2$ as a function of $x$: ○, ●, Hf; □, ■, Ti; ◇, ◆, Nb; ○, □, ◇, discharge current of 20 mA $g^{-1}$; ●, ■, ◆, discharge current of 70 mA $g^{-1}$.

very favorably with the other metal hydrides cited in the literature [6,31]. At the relatively higher discharge current of 70 mA (g alloy)$^{-1}$, there is a large drop in discharge capacity for most alloys. However, the two alloys having the pure C14 phase ($NbM_2$ and $Zr_{0.5}Ti_{0.5}M_2$) do not show a drop in capacity. Also, the capacity drop is quite small for the alloys having a b.c.c. phase ($Zr_{0.25}Ti_{0.75}M_2$ is 89% C14 and 11% b.c.c.; $TiM_2$ is 100% b.c.c.).

By comparing the theoretical and measured discharge capacities, a better understanding of the effect of higher discharge current on discharge capacity can be achieved. The theoretical discharge capacity $C_{th}$ is obtained from the relation

$$C_{th}(\text{mA h g}^{-1}) = \frac{F[\text{H}]/[\text{M}]}{3.6M_{av}} \quad (3)$$

where $F$ ($9.6487\times10^4$ C mol$^{-1}$) is the Faraday constant, [H]/[M] is the hydrogen-to-metal atom ratio, and $M_{av}$ is the average atomic weight of the alloy. We arbitrarily choose 5 MPa as the reference pressure to determine the [H]/[M] value, because it is near the maximum pressure reached and, for most alloys, the ratio [H]/[M] is near saturation at this pressure.

In Fig. 10 we present the ratio of the measured discharge capacity over the calculated discharge capacity for the systems $Zr_{1-x}Ti_xM_2$, $Zr_{1-x}Nb_xM_2$ and $Zr_{1-x}Hf_xM_2$. Fig. 10(a) shows that the $Zr_{1-x}Ti_xM_2$ alloys which are a mixture of C15 and C14 phases ($x=0$ and 0.25) show a significant drop in discharge capacity when the discharge current is increased. On the contrary, the alloy with the pure C14 phase ($x=0.5$) does not show any drop in capacity while the pure b.c.c. alloy ($x=1$) presents a small drop in capacity. It is hard to obtain a definitive explanation for this behavior. One possibility is that, for this system, the C14 phase in itself shows a higher discharge capacity at a high discharge current than does the C15 phase. Another explanation is that the interaction at the boundary between C14 and C15 phases is responsible for the drop in discharge capacity at high current. Also, because the surface of the Laves phase alloys differs from that of $AB_5$-type alloys, it is expected that surface effects on the kinetics in the Laves phase are different from $AB_5$-type alloys.

Fig. 10(b) presents the system $Zr_{1-x}Nb_xM_2$. The ratio of the measured to the theoretical discharge capacity decreases from $x=0$ to $x=0.5$ and increases for $x=0.75$. However, from $x=0$ to $x=0.75$ the discharge capacity decreases from 420 to 85 mA h $g^{-1}$ at a low discharge current. At a high discharge current the discharge capacity decreases from 215 to 62 mA h $g^{-1}$. Because of this important decrease in discharge capacity, we think that Fig. 10(b) should be viewed with great caution and that it is hard to see a general trend with such small values.

The system $Zr_{1-x}Hf_xM_2$ is shown in Fig. 10(c). At a high discharge current, the ratio of the measured to the theoretical discharge capacity steadily increases from $x=0$ to $x=1$. On the contrary, at a low discharge current, this ratio is constant. From Fig. 2 we see that, in this system, the proportion of C14 phase increases from $x=0$ to $x=0.5$ and is constant from $x=0.5$ to

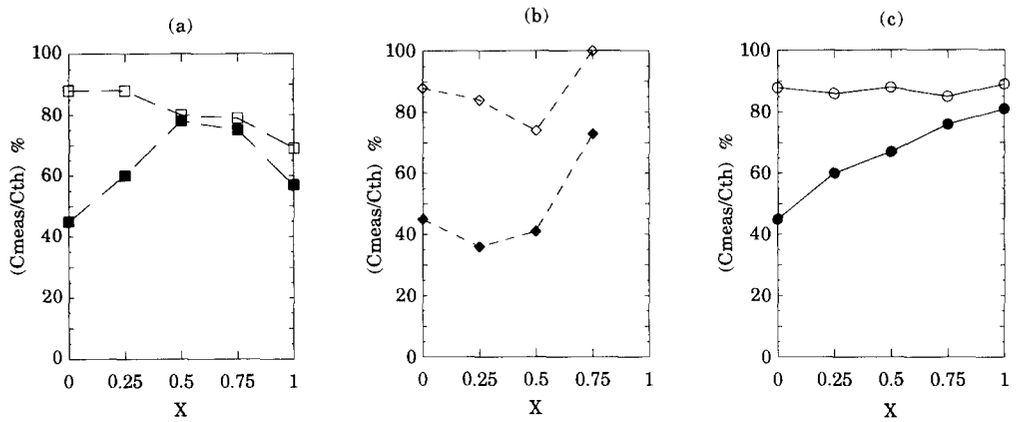


Fig. 10. Ratio of the measured discharge capacity to the calculated discharge capacity for the $Zr_{1-x}A_xM_2$ system for discharge currents of 20 mA $g^{-1}$ (□, ◇, ○) and 70 mA $g^{-1}$ (■, ◆, ●): (a) $Zr_{1-x}Ti_xM_2$; (b) $Zr_{1-x}Nb_xM_2$; (c) $Zr_{1-x}Hf_xM_2$.

$x = 1$. Consequently, we conclude that, at a low discharge current, the increase in the ratio of the measured to the theoretical discharge capacity is due partly to the higher content of C14 phase and partly to the substitution of the Zr atom by the Hf atom.

## 4. Conclusion

In this work, by the Rietveld method we have estimated the phase abundance of the alloys. We found that two Laves phases can coexist for a wide variation of the A site for the $Zr_{1-x}A_xM_2$ system (A ≡ Ti, Hf or Nb). The presence of the C15 phase seems to be related to the bond distance between two M site atoms. The phase stability under hydriding has been established. From PC isotherm measurements, we observe that multiphase alloys act as a single phase. For the system $Zr_{1-x}Ti_xM_2$, there is a smooth transition from the Laves phase to the b.c.c. solid solution phase. Also, we find that the b.c.c. phase is a hydrogen absorber. For battery application, in the system $Zr_{1-x}Ti_xM_2$, the alloys with the C15 phase present a large reduction in discharge capacity when the discharge current is increased. For the alloys composed of only the C14 phase, the discharge capacity does not change significantly when the discharge current is increased.

## Acknowledgments

The authors with to thank Mr. M. Yoshida of the Hitachi Chemical Co. Ltd. and Mr. H. Iba of the Toyota Motor Corporation for helpful discussions. Thanks are due to Mr. K. Nomura of the National Institute of Materials and Chemical Research for his help in measuring the PC isotherms. J. Huot is supported by an STA Fellowship of the Science and Technology Agency of Japan.

## References

[1] F.E. Lynch, *J. Less-Common Met., 172–174* (1991) 943.
[2] J.J. Willems, *Philips J. Res., 39* (1984) 1.
[3] T. Sakai, H. Yoshinaga, H. Miyamura, N. Kuriyama and H. Ishikawa, *J. Less-Common Met., 180* (1992) 37.
[4] H. Sawa, M. Ohta, H. Nakano and S. Wakao, *Z. Phys. Chem. NF, 164* (1989) 1527.
[5] Y. Moriwaki, T. Gamo, A. Shintani and T. Iwaki, *Denki Kagaku, 57* (1989) 488.
[6] Y. Moriwaki, T. Gamo, H. Seri and T. Iwaki, *J. Less-Common Met., 172–174* (1991) 1211.
[7] K. Kanematsu, *J. Phys. Soc. Jpn., 27* (1969) 849.
[8] A.F. Wells (ed.), *Structural Inorganic Chemistry,* Oxford University Press, Oxford, 1984.
[9] R.P. Elliott and W. Rostoker, *Trans. Am. Soc. Met., 50* (1958) 618.
[10] D.G. Ivey and D.O. Northwood, *Z. Phys. Chem. NF, 147* (1986) 191.
[11] S.R. Ovshihsky, M.A. Fetcenko and J. Ross, *Science, 260* (1993) 176.
[12] D. Shaltiel, I. Jacob and D. Davidov, *J. Less-Common Met., 53* (1977) 117.
[13] H. Fujii, V.K. Shinha, F. Pourarian and W.E. Wallace, *J. Less-Common Met., 85* (1982) 43.
[14] T. Riesterer, P. Kofel, J. Osterwalder and L. Schlapbach, *J. Less-Common Met., 101* (1984) 221.
[15] A. Suzuki and N. Nishima, *Mater. Res. Bull., 19* (1984) 1559.
[16] I. Yonezu, S. Fujitani, A. Furukawa, K. Nasako, T. Yonesaki, T. Saito and N. Furukawa, *J. Less-Common Met., 168* (1991) 201.
[17] H. Oesterreicher and H. Bittner, *Mater. Res. Bull., 13* (1978) 83.
[18] V.K. Sinha, F. Pourarian and W.E. Wallace, *J. Less-Common Met., 87* (1982) 283.
[19] K. Nomura, H. Uruno, S. Ono, H. Shinozuka and S. Suda, *J. Less-Common Met., 107* (1985) 221.
[20] F. Izumi, in R.A. Young (ed.), *The Rietveld Method,* Oxford University Press, Oxford, 1993, Chapter 13.
[21] R.A. Young, in R.A. Young (ed.), *The Rietveld Method,* Oxford University Press, Oxford, 1993, Chapter 1.
[22] R.A. Young and E. Prince, *J. Appl. Crystallogr., 15* (1982) 357.
[23] E. Prince, in R.A. Young (ed.), *The Rietveld Method,* Oxford University Press, Oxford, 1993, Chapter 3.
[24] R.J. Hill, *Powder Diffr., 6* (1991) 74.

[25] E.A. Brandes and G.B. Brook (eds.), *Smithells Metals Reference Book*, Butterworth–Heinemann, Oxford, 1992.
[26] E. Piegger and R.S. Craig, *J. Chem. Phys., 39* (1963) 137.
[27] A. Simon, *Angew. Chem., Int. Edn. Engl., 22* (1983) 95.
[28] R.L. Snyder, in R.A. Young (ed.), *The Rietveld Method*, Oxford University Press, Oxford, 1993, Chapter 7.
[29] D.P. Schoemaker and C.B. Schoemaker, *J. Less-Common Met., 68* (1979) 43.
[30] R. Griessen and T. Riesterer in L. Schlapbach (ed.), *Hydrogen in Intermetallic Compounds I*, Springer, Berlin, 1988.
[31] G. Sandrock, S. Suda and L. Schlapbach, in L. Schlapbach (ed.), *Hydrogen in Intermetallic Compounds II*, Springer, Berlin, 1992, Chapter 5.